Publ. Astron. Soc. Aust., 1998, 15, 309–17

A Statistical Comparison of Line Strength Variations in Coma and Cluster Galaxies at $z \sim 0{\cdot}3$

Lewis A. Jones and Warrick J. Couch

School of Physics, University of New South Wales, NSW 2052, Australia
lewis@edwin.phys.unsw.edu.au

Received 1997 December 29, accepted 1998 August 20

Abstract: We present a statistical comparison between spectral line strength variations in Coma galaxies and galaxies in three rich clusters at $z \sim 0{\cdot}3$. Using a principal component analysis, we have transformed the observable quantities, the line strengths, into new mutually orthogonal axes and found two specific results. First, more independent parameters are required to account for the line strength variations in the distant cluster data than in the Coma data, and second, line strengths which are *not* correlated in the distant cluster data are strongly coupled in the Coma data. These results suggest that galaxies in clusters have been homogenised such that most of the information from the conditions present at their formation has been destroyed. Hence, it may be possible that the present-day homogeneity of early-type galaxy properties, e.g. the fundamental plane relation, does not require a single formation scenario, but that a variety of formation scenarios for different galaxies could still yield the observed behaviour of nearby galaxies.

Keywords: galaxies: individual (Coma, AC103, AC114, AC118) — galaxies: clusters — galaxies: evolution — galaxies: formation — methods: data analysis

1 Introduction

Early-type galaxies have long been known to exhibit strong systematic behaviour in many of their photometric properties. This behaviour manifests itself in several ways, for example, the colour–absolute magnitude relation (Visvanathan & Sandage 1977) and the fundamental plane relations (Faber & Jackson 1976; Dressler et al. 1987; Djorgovski & Davis 1987). The tight correlations among many different photometric properties of early-type galaxies and yet the relatively small number of parameters required to describe their behaviour suggest a similar origin and evolutionary history for early-type galaxies. Observations of distant clusters show that the colour–absolute magnitude relation is well formed at $z \sim 0{\cdot}5$ (Ellis et al. 1997), placing even tighter constraints on the origin of the homogeneity of the photometric properties of early-type galaxies.

On the other hand, it is not clear that broadband photometry can provide any *unambiguous* indicators of the star formation and chemical enrichment history in a galaxy without our being able to fix the age or the metallicity via other means. Because of the degeneracy of age and metallicity of broadband colours in old stellar populations (Worthey 1994), it is only under the *assumption* that all early-type galaxies are old and stopped forming stars a long time ago that the colour–absolute magnitude relation becomes a simple sequence in metallicity.

When we turn to spectroscopy, the picture changes. We see in studies such as those of O'Connell (1976), Rose (1985a 1985b, 1994), González (1993) and Jones (1996) that for a narrow range of photometric properties, in both single stellar populations and galaxies, there are large variations in spectral line strengths. The line strength variations relate directly to differences in the underlying stellar populations, giving cause to question the single-origin interpretation for early-type galaxies derived from the broadband photometric relations. Hence, spectroscopy provides a way to break through the ambiguity of broadband colours and place tighter constraints on the formation and evolutionary processes of early-type galaxies.

However, integrated spectroscopy of galaxies at the present epoch has an inherent ambiguity of its own because integrated galaxy light is just that, *integrated*, so the properties derived from such a study will always be luminosity-weighted averages of the different constituent stellar populations, and even multi-wavelength studies of galaxies have yet to uniquely identify all of the contributors to the integrated light. For this reason, we need to observe, directly, intermediate stages of galaxy evolution which can act as signposts to direct us from the period of formation to the present day. Not only will these direct observations tell us how galaxies are changing in time, but they will act as stakes in the ground to constrain galaxy formation models,

 1323-3580/98/030309$05.00

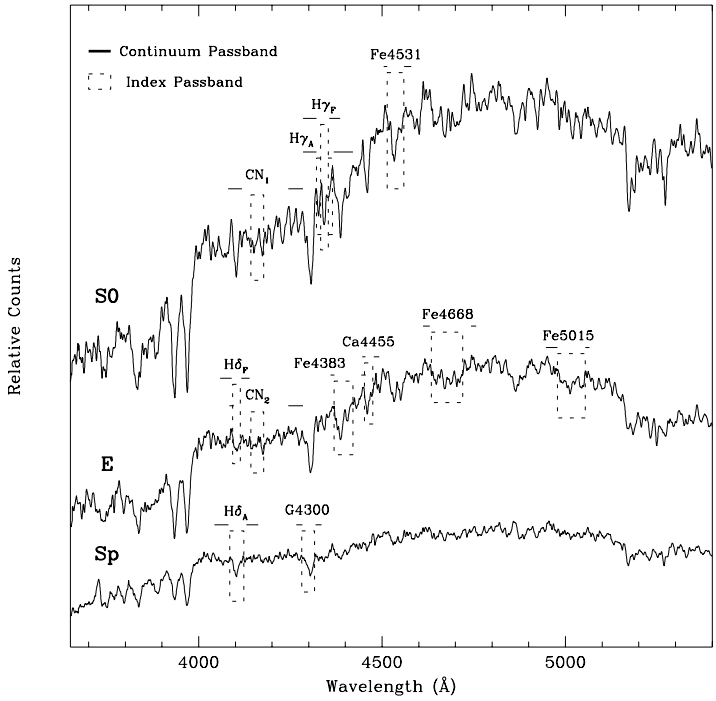

Figure 1—Qualitative presentation of the index and continuum passbands for the 12 spectral indices defined in this paper. The passbands are overlayed on three composite spectra from the distant cluster sample of galaxies. The scale on the y-axis is in relative counts.

so that one day models will have to reproduce quasar absorption systems, morphological number counts of galaxies, the galaxy luminosity function, and present-day observations of galaxy populations, as well as the integrated spectroscopic properties of the intermediate stages of galaxy evolution.

As a first step towards this goal, we have undertaken a spectroscopic comparison between galaxies in a nearby rich galaxy cluster and three similarly rich clusters at $z \sim 0{\cdot}3$. In this paper we present a statistical analysis of the spectral variations in the distant cluster galaxies relative to the nearby galaxies, concentrating on what type of information can be derived from the sample, with a full discussion of the implications for the galaxy stellar populations to await a future article. Section 2 describes the sources of the data, Section 3 presents the analysis, and Section 4 is a discussion of the results.

2 Data

The data used in our analysis were taken from previously published work; the purpose of this section is therefore only to give information about the data relevant to the goals of this paper.

The distant cluster data were taken from the studies of Couch & Sharples (1987; hereafter CS), Couch et al. (1994), and Couch et al. (1998). The data of CS were taken at the $3{\cdot}9$ m Anglo-Australian Telescope (AAT) with the FOCAP multi-fibre spectrograph and the IPCS detector in August and September 1985, and have a spectral resolution of ∼4 Å FWHM. The Couch et al. (1994) and Couch et al. (1998) data were also taken at the AAT using the multi-slit Low Dispersion Survey Spectrograph (LDSS-1) and have a spectral resolution of ∼9 Å FWHM. In total, 249 galaxy spectra are available, providing 147 radial velocity members between the three clusters. Of these, 95 have Hubble-type classifications based on high-resolution imaging taken with the Wide Field and Planetary Camera (WFPC) by HST (Couch et al. 1998).

The Coma cluster data have been published by Caldwell et al. (1993) and Caldwell & Rose (1997), and the reduced galaxy spectra were kindly provided by these authors for this work. They consist of spectra for 63 elliptical, 120 S0, 4 spiral, and 3 unclassified galaxies at a resolution of ∼4 Å FWHM. All of the Coma spectra are cluster members.

The rest-frame wavelength coverage of nearly all the spectra is $3900 \leq \lambda \leq 5300$ Å, i.e. from the CaII H & K lines through to the Mg triplet. All of the galaxy spectra have been smoothed to the 9 Å resolution of the LDSS-1 data to avoid any systematic effects in measuring the spectral indices.

3 Analysis

3.1 Spectral Indices and Errors

As a means of characterising the spectra described in Section 2, we have measured 12 pseudo-equivalent widths for 9 different strong absorption features in each galaxy spectrum. The pseudo-equivalent widths, which we will call spectral indices, are computed using the ratio of the flux in a 30–

https://doi.org/10.1071/AS98309 Published online by Cambridge University Press

Table 1. Definitions of spectral indices

Index name	Index passband (Å)	Continuum (Å) Blue	Red	1σ errors (Å) High-z	Coma
CN_1	4142·125 4177·125	4080·125 4117·625	4244·125 4284·125	1·6223	0·2134
CN_2	4142·125 4177·125	4083·875 4096·375	4244·125 4284·125	1·5911	0·4676
G4300	4281·375 4316·375	4266·375 4282·625	4318·875 4335·125	1·5784	0·3694
Ca4455	4452·125 4474·625	4445·875 4454·625	4477·125 4492·125	1·3575	0·5056
Fe4383	4369·125 4420·375	4359·125 4370·375	4442·875 4455·375	1·9135	0·6284
Fe4531	4514·250 4559·250	4504·250 4514·250	4560·500 4579·250	1·7801	0·6706
Fe5015	4977·750 5054·000	4946·500 4977·750	5054·000 5065·250	2·6780	0·4683
Hδ_A	4084·750 4123·500	4042·850 4081·000	4129·750 4162·250	1·6582	0·2377
Hδ_F	4092·250 4113·500	4058·500 4089·750	4116·000 4138·500	1·2007	0·2178
Hγ_A	4321·000 4364·750	4284·750 4321·000	4368·500 4421·000	1·9689	0·2449
Hγ_F	4332·500 4353·500	4284·750 4321·000	4356·000 4386·000	1·3432	0·1969
Fe(C_2)4668	4634·000 4720·250	4611·500 4630·250	4742·750 4756·500	2·4559	0·5715

40 Å index passband to a continuum defined by connecting a straight line between the average flux levels in a red and blue sideband, each also ∼30–40 Å wide. This type of spectral index has been used extensively by the Lick group (Wood 1969; Faber 1973; Gorgas et al. 1993; González 1993; Worthey 1994); a list of all but the Balmer indices has been compiled by Worthey (1994). The four Balmer indices included here were defined in Worthey & Ottaviani (1997). Figure 1 gives a qualitative picture of the index definitions overlayed on three composites of galaxy spectra from the distant cluster data, and Table 1 gives the wavelength definitions of the indices and the average 1σ error for each index. The three data sets considered here were all collected with different telescope–instrument–detector combinations, and in an effort to make the most consistent error estimates possible, we have chosen to use pure photon statistics to determine the errors in the spectral indices, relying only on the number of counts per pixel in the spectra. The flux in each index band was computed as

$$F_i = \frac{\Sigma F_{i,k}/\sigma^2_{i,k}}{\Sigma 1/\sigma^2_{i,k}} ,$$

where F_i is the summed flux for index i, $F_{i,k}$ is the flux at point k for index i, and $\sigma_{i,k}$ is its Poisson error bar. The cumulative error bar for an index passband was computed as

$$\sigma^2_i = \frac{1}{\Sigma 1/\sigma^2_{i,k}} .$$

The flux in each continuum band and associated errors were computed in exactly the same manner as for the index passbands.

A source of uncertainty in the comparison of index measurements *between* the three data sets (FOCAP, LDSS-1, and Hydra) is differences in continuum shape. As long as the slope of the continuum within each data set is constant, or changing in the same sense relative to the other data sets, over the wavelength range of the index (plus continuum bands) there will be no effect on the relative strengths of the index measurements. However, if the continuum slopes are changing relative to one another in the three data sets, there can be systematic shifts in the index strengths between the data sets. In order to minimise this potential systematic shift, we have determined the relative spectral response functions of the three data sets and normalised all the data sets to the spectral response of the IPCS data from CS. To determine the transformation from the LDSS-1 data to the IPCS response, we formed a ratio of the average spectra of ten galaxies common to both samples and made a smooth fit to that ratio. To go from Hydra to the IPCS response, we averaged all the E and S0 spectra from IPCS, and again for Hydra, formed a ratio of those mean spectra, and fit the ratio.

A second source of uncertainty in comparing the data sets is the difference in physical dimension being sampled in the Coma and high-redshift galaxies. While the the Coma data are looking only at the galaxy nuclei, the high-redshift data are looking at a much more global aspect of the galaxies. The question to be addressed then is whether, within the uncertainties in the high-redshift data, the differences we expect from line strength gradients within the galaxies will be detectable, and hence, produce a systematic offset between the data sets. Although there will always be pathological cases, we confine our answer to the general trends observed in other studies. Perhaps the simplest and most extensive study of line strength gradients in early-type galaxies is in the PhD thesis of Jesus González (1993). He has not computed gradients for all the same indices as are presented in this paper, so we use his Hβ gradients to compute the expected changes in our higher-order Balmer lines Hγ and Hδ, and we use his average Fe gradient to compute the expected changes in our average Fe index (his average Fe index contains the same individual Fe indices as ours plus others). González's average Hβ gradient is

https://doi.org/10.1071/AS98309 Published online by Cambridge University Press

$$\frac{\Delta\log(\mathrm{H}\beta)}{\Delta\log(r)} = 0{\cdot}013\,,$$

and for Fe it is

$$\frac{\Delta\log\langle\mathrm{Fe}\rangle}{\Delta\log(r)} = 0{\cdot}070\,.$$

At the distance of Coma (with $H_0 = 50$) $1'' = 0{\cdot}34$ kpc, while in the distant clusters ($z = 0{\cdot}31$) $1'' = 6{\cdot}07$ kpc. The Hydra fibres for the Coma data were $2''$ in diameter, the LDSS-1 slit width was $1.''5$, and the FOCAP fibre diameter was $2.''6$. In Coma the $1''$ radius is $0{\cdot}34$ kpc, and taking the larger diameter of the FOCAP fibres, the high-redshift observations extend out to $7{\cdot}89$ kpc. This predicts a change of $0{\cdot}050$ in Hδ and $-0{\cdot}964$ in Fe, whereas the typical uncertainties in those indices are $1{\cdot}430$ and $2{\cdot}124$ respectively. Hence the changes in the measured index values in the high-redshift data relative to the Coma data would be undetectable due to the measurement uncertainties.

Given the extensive descriptions of the spectral indices available in the literature, and the fact that we have concentrated on a statistical analysis of the spectra as opposed to a detailed investigation of the stellar populations, we give only a brief discussion of the individual indices used here. For a full description of the spectral indices and their use in integrated light studies, the reader should refer to Worthey (1994), Worthey & Ottaviani (1996) and Jones (1996).

• **CN$_1$** & **CN$_2$** These two indices both straddle the CN bandhead at 4216 Å, and they share the same index passband, but have a different blue continuum band. The index response is nearly flat for dwarf stars of all temperatures and giants with $T_{eff} \geq 4500$ K, but shows gravity and metallicity sensitivity below $T_{eff} \leq 4500$ K.

• **G4300** This index measures the G-band of CH at 4300 Å and shows mostly gravity and temperature sensitivity.

• **Ca4455** This index measures the only strong CaI feature in this region of the spectrum. It is mostly sensitive to temperature and metallicity.

• **Fe4383**, **Fe4531** & **Fe5015** These indices all measure prominent Fe absorption features. They are mostly sensitive to temperature and metallicity, but also show gravity sensitivity for G stars.

• **Hδ_A** & **Hδ_F** These two indices are broad and narrow definitions respectively for the Hδ Balmer line. Balmer lines are generally temperature-sensitive in all stars.

• **Hγ_A** & **Hγ_F** Similar to Hδ above, these are broad and narrow definitions for the Hγ Balmer line. Again, these indices show mostly temperature sensitivity, although there is significant metallicity sensitivity in this definition of the Hγ index.

• **Fe(C$_2$)4668** Originally denoted Fe4668, this index measures the strong absorption at 4668 Å. There is an Fe feature there, but it has been shown that the strength of the absorption is mostly a function of the molecular carbon bands at the same location (Tripicco & Bell 1995). Accordingly, the index is sometimes now denoted C$_2$4668. It shows strong metallicity sensitivity, as well as gravity sensitivity.

3.2 Principal Component Analysis

We have carried out a principal component analysis (PCA) of the distant cluster and Coma data in order to quantify the line strength distributions in the nearby and distant cluster galaxies. A principal component analysis transforms the observable axes, in this case the spectral line strengths (which are necessarily interdependent, e.g. all partially temperature sensitive), into a new set of axes, or components, which are mutually orthogonal. This is accomplished by choosing each new axis to maximise the total variance along that axis. Hence, the PCA acts as a means of data compression by bringing together in a single new axis correlations between several different observables, so that the most significant few principal components will describe all of the real variations in the data while the rest of the components will contain mostly uncorrelated noise. Each new axis is a linear combination of the observable axes and is associated with an eigenvalue, which is a measure of the fraction of the variation in the observables accounted for in that new axis.

For the PCA, in order to ensure a more meaningful comparison between the data sets, we have effected two further changes to the galaxy data. First, we have restricted both the Coma and high-redshift samples to include only the morphologically classified E and S0 galaxies. This leaves 40 galaxies in the high-reshift sample and 183 in the Coma sample. Second, we have degraded the Coma data to the same signal-to-noise ratio as the high-redshift data. This was done by adding Poisson noise and Gaussian read noise to the Coma spectra with the IRAF task MKNOISE until the RMS scatter in the wavelength region $\lambda\lambda$3785–3835 divided by the average flux over that range was the same as in the high-redshift data.

Of the 12 spectral indices measured, there are 3 pairs of indices where each index in the pair is a different measurement of the same feature. Those pairs are Hδ_A and Hδ_F, Hγ_A and Hγ_F, and CN$_1$ and CN$_2$, which each cover the CN bandhead at 4216 Å. There are also three different iron features, Fe4383,

https://doi.org/10.1071/AS98309 Published online by Cambridge University Press

Fe4531 and Fe5015. A single index is formed for each of the above sets of like indices by forming the weighted average of the indices in each set, so that out of the 12 original measurements, seven indices are input into the PCA code. The weighted averages were computed as

$$I_{i,j} = \frac{\Sigma I_{i,k}/\sigma_{i,k}^2}{\Sigma 1/\sigma_{i,k}^2} ,$$

where $I_{i,j}$ is the summed index value j for galaxy i, $I_{i,k}$ is the individual index k for galaxy i, and $\sigma_{i,k}$ is its associated error. The errors for the new summed indices were computed as

$$\sigma_{i,j}^2 = \frac{1}{\Sigma 1/\sigma_{i,k}^2} .$$

It is then those 7 summed indices which are transformed, through the PCA, into 7 new orthogonal axes. For reasons described in the next section, the PCA was run in two incarnations: first, on the high-redshift, clean Coma, and noisy Coma samples independently, producing three sets of new axes, or eigenvectors, which are each *different* linear combinations of the original spectral indices; and second, on a combined sample of high-redshift and noisy Coma galaxies, producing a single set of eigenvectors describing the entire sample. The combined run was conducted with a random sample of 40 Coma galaxies selected to have the same morphological mix as the high-redshift sample. This was done so that the principal components would not be artificially dominated by the Coma spectra due to the larger number of Coma galaxies. Table 2 shows the eigenvalues from the run of the separate samples, and Table 3 shows the eigenvectors from the combined run. With the new set of independent axes, we will now look at how to relate them to the physical state of the cluster galaxies.

Table 2. Eigenvalues for the high redshift, noisy Coma, and Coma samples

PC	High-z	Noisy Coma	Coma
1	2·1649(30·9)[A]	3·3646(48·1)	3·4427(49·2)
2	1·5421(22·0)	0·8662(12·4)	1·1842(16·9)
3	1·1843(16·9)	0·8314(11·9)	0·6807(9·7)
4	0·9724(13·9)	0·6616(9·5)	0·5605(8·0)
5	0·4547(6·5)	0·5540(7·9)	0·4751(6·8)
6	0·3725(5·3)	0·4334(6·2)	0·3572(5·1)
7	0·3091(4·4)	0·2887(4·1)	0·2995(4·3)

[A] Numbers in parentheses are the percentage variation of the sample accounted for by that eigenvalue.

4 Results

In this section we briefly address two questions; first, how many parameters are required to adequately describe the galaxy spectra, and second, what physical phenomena are associated with the new axes. Because of the data compression property of PCA, it is an ideal method for investigating the first question. Although a physical description of the new axes will not often be immediately apparent, the *number* of principal components that contain most of the information in the spectra tells us how many different parameters are needed to fully describe the data set, in this case, the galaxy line strengths.

Figure 2 shows the eigenvalues for the three different samples: empty squares for the clean Coma data, filled squares for the noisy Coma data, and filled circles for the high-redshift data. As the components, or eigenvectors, represented by the eigenvalues are different for each different data set, no direct comparison of the properties of the components themselves can be made, but we are for the moment only interested in the number of components required to describe the data set, and this individual analysis of the data sets *will* tell us that. Remembering that the eigenvalues show the amount of the total sample variance accounted for in that principal component, this diagram displays the distribution of variances in the new axes for each of the three samples. One feature of the diagram that is clear at a first look is the difference in the shape of the distribution of the variances in the Coma data relative to the high-redshift data. The

Table 3. Eigenvectors for the Coma plus high-z cluster sample

Index	PC1	PC2	PC3	PC4	PC5	PC6	PC7
CN	−0·3739	−0·4144	0·4610	−0·1038	−0·3148	0·3440	−0·4978
CH	−0·4629	−0·2203	−0·4818	−0·0796	0·0652	0·5490	0·4395
Ca	−0·3750	0·4977	−0·1162	0·3392	0·4646	0·1671	−0·4892
Fe	−0·0215	−0·6897	0·0263	0·2830	0·6012	−0·2850	−0·0216
Hδ	0·3179	−0·1988	−0·4740	0·5995	−0·4258	0·1316	−0·2770
Hγ	0·5059	0·0485	0·4076	0·2087	0·2724	0·6494	0·1900
C_2	−0·3845	0·1207	0·3879	0·6203	−0·2528	−0·1792	0·4543
Eig.[A]	30·3	21·7	16·6	13·8	6·5	5·8	5·3
F test[B]	$< 1\%$	$< 1\%$	2·5%	15%	100%	100%	100%

[A] Eigenvalues are shown as a percentage of the total variance of the sample accounted for in that principal component.
[B] F test percentages represent the chance that uncertainties in the index measurements alone can account for the variance in the principal component, i.e. a low percentage indicates a high significance for that component.

https://doi.org/10.1071/AS98309 Published online by Cambridge University Press

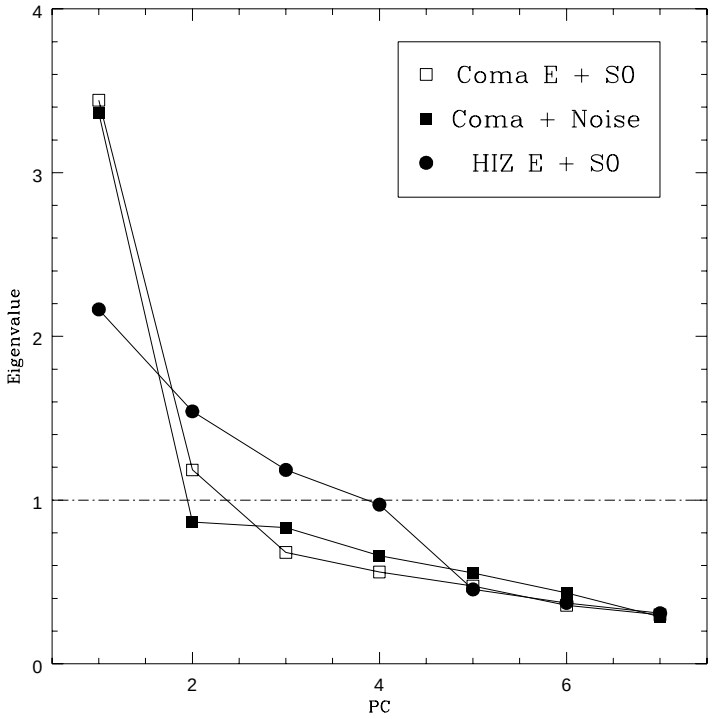

Figure 2—This figure demonstrates the main result. It shows the distribution in line strength variations contained in each principal component for the clean Coma, noisy Coma, and high-redshift data. The open squares represent the clean Coma data, filled squares represent the noisy Coma data, and filled circles represent the high-redshift sample. The dot–dashed line shows the eigenvalues for a sample of 100% uncorrelated variances. Taking the shallow trend of the Coma eigenvalues as the benchmark of components containing nearly no spectral information, it follows that, at most, two components in the Coma data are required to describe most of the line strength variation there, while the high-redshift data requires four components to explain the line strength variations in that data set.

first component in the Coma data contains 3 to 4 times (clean and noisy, respectively) the variance of the second component, while the first high-redshift component contains less than 1·5 times the variance of the second. Then, while the coma eigenvalues flatten out, the high-redshift eigenvalues continue on the same, more moderate, trend as for the first two until at the fifth component, it joins the already shallow trend of the Coma data.

Although the trends for the clean and noisy Coma samples are strikingly similar, and suggest that differences between the high-redshift and Coma line strengths are *not* due to the higher noise of the distant cluster data, the differences between the two Coma samples are also instructive. What is immediately apparent is that the variance in the first two components of the noisy data has lessened while the rest of the components have picked up some of the overall sample variance. If the two samples were identical except for the noise characteristics, then one would expect the trend to become more shallow for the first two components and steepen for the latter ones, hence becoming more like the high-redshift data. However, the trend becomes even steeper in the *noisy* data for the first two components. In adding the noise, we have added uncorrelated information to the spectra at all wavelengths. This process will necessarily mask some of the stronger correlations in the data, and remove power from the components associated with those correlations, while adding power to the components which already represent mostly uncorrelated noise. This provides a way to distinguish components that contain the strong correlations from those containing mostly noise. Using this criterion, Figure 2 tells us that the first two components of the Coma data contain most of the information and the latter five are mostly noise.

While we have not degraded the high-redshift data and therefore do not have the same criterion available to us, the dot–dashed line represents the value of the eigenvalues for a sample of 100% uncorrelated variances, and can act as a different type of benchmark. Because of the fact that we see the five latter Coma components move almost uniformly toward the line of 100% uncorrelated variances when noise is added, we will take that trend to define the behaviour of components containing mostly the uncorrelated contributions to the sample variance. We can say then that the first four high-redshift components are not uncorrelated noise as they do not lie on that trend. Taking the shape of the distributions of the variances together with the response of the components to adding noise, we

https://doi.org/10.1071/AS98309 Published online by Cambridge University Press

Table 4. Correlations and KS probabilities for the combined sample

Index name	PC1 High-z[A]	PC1 Coma[B]	PC1 KS[C]	PC2 High-z	PC2 Coma	PC2 KS
CN	9	1	7	7	<1	<1
CH	<1	<1	<1	94	4	<1
Ca	<1	8	<1	<1	15	<1
Fe	31	3	<1	<1	<1	<1
Hδ	2	87	1	20	63	<1
Hγ	<1	<1	<1	44	49	<1
C_2	2	<1	1	16	25	<1

[A] Percentage chance that correlation could result from a random distribution.
[B] Same as for high-z.
[C] Percentage chance that the two distributions could be drawn from the same parent population.

can now answer the first question by saying that *for the three rich clusters at $z \sim 0{\cdot}3$ discussed in this paper, more parameters are required to describe their spectral line strength variations than for the nearby Coma cluster*. Specifically, there are four independent parameters present in the high-redshift data, against only two in the Coma data.

For the purpose of addressing the question of the physical significance of the principal components, we turn to the second PCA run with the combined-clusters data set described in Section 3.2. This allows us to compare the distant clusters and Coma using the same set of basis vectors, the common principal components. Table 3 shows the eigenvectors for the combined run, the eigenvalues (shown as % variance), and the F-test probability that the eigenvector in question could be fully explained by measurement uncertainties, i.e. low probability means high significance. The eigenvector elements in Table 3 are actually correlation coefficients and range from +1 for a complete positive correlation of galaxy weights with index value, through 0 for no correlation, to −1 for a complete anticorrelation; the degree of correlation is the degree to which variations in that index are responsible for the variations in the component. From the F-test probabilities in Table 3 it can be seen that only the first two principal components are significant to better than 99%. The increasing noise in the rest of the components will weaken any conclusions drawn about their relationship to physical quantities, so for this reason we confine our discussion to the properties of the first two components.

Each principal component is a linear combination of the original set of 7 spectral indices, the coefficients of which are contained in the eigenvectors (the correlation coefficients). The index values for any galaxy can then be reconstructed exactly from the eigenvectors by multiplying each of the seven eigenvectors by an appropriate weight; hence a weight quantifies the significance of a given eigenvector in describing a particular galaxy spectrum. Comparing the distribution of weights in the combined sample with the index values themselves can tell us about the physical meaning of the principal components.

To that end, using the weights generated with the common eigenvectors, we have computed the correlations of weight versus index value for the two samples individually, as well as the two-dimensional KS-test probabilities of the weight versus index value distributions for each sample. Table 4 shows those results. The correlation probabilities are shown as the percentage chance that the measured correlations could result from a random distribution, and the KS probabilities are shown as percentage chances that the two distributions (weight versus index value for each of the Coma and high-z samples) could be drawn from the same parent population. For the correlation probabilities then, a low value indicates a high significance to the correlation, and for the KS probabilities, a low value indicates the distributions are different. One simple result we can draw from the KS probabilities in Table 4 is that the two samples are overwhelmingly different in the relationship between their line strengths and both of the first two principal components. Hence, *Coma and the high-redshift clusters are spectroscopically different.*

Some of the ways in which they are different can be seen in the correlations of index value versus PC weight. For the first component, each index is well correlated with at least one of the cluster samples and, from Table 3, we see that the strongest correlation is with Hγ. However, the strong correlation may be due to the particular metallicity sensitivity of this definition of the index (see Section 3.1), related to its proximity to the G-band. For this reason, it will be prudent to regard Hγ as more of a psuedo-metal line than a Balmer line. However, regardless of the origin of the correlation of the first component with Hγ, we also have Hδ, which is more free from metal contamination, so we rely on that Balmer line for an indication of the general behaviour of Balmer lines.

The difference in the response of each sample to the first component is interesting. From Table 4, we see that in Coma, Hδ does not contribute to the first component (weak correlation), which makes the first component a general indicator of metal line

https://doi.org/10.1071/AS98309 Published online by Cambridge University Press

strengths. For the high-redshift clusters, Hδ does contribute, while Fe does not, so Hδ and the light elements are important for the first component in the high-redshift clusters. In the second component, the Balmer lines show only weak correlations, while both samples are strongly correlated with Fe, showing that in both environments there is at least one physical factor, unrelated to the Balmer line strengths, which drives the heavy-element line strengths.

The spectroscopic differences between Coma and the high-redshift sample are real and their interpretation will provide an insight into galaxy evolution in rich cluster environments. We briefly address the question of interpretation below.

5 Discussion

We have made a statistical comparison of spectral line strengths in three rich galaxy clusters at $z \sim 0{\cdot}3$ with those in the nearby Coma cluster. Using the morphological information from Hubble Space Telescope images and a principal component analysis to analyse the relationships between spectral line strengths in the nearby and distant clusters, we have found two specific results.

First, more independent parameters are required to account for the line strength variations in the distant cluster data than in the Coma data. Couch & Sharples (1987) have demonstrated that the colour–magnitude diagrams of these clusters show little scatter in their early-type galaxy populations, and the same has been shown for Coma by Colless & Dunn (1996). In conjunction with the small photometric scatter of the early-type galaxies in both the distant clusters and Coma, the change in spectroscopic properties between the distant clusters and Coma serves to confirm the ambiguity of broadband colours for investigating the star formation histories of galaxies. Although this is not a surprise, it should be considered as yet another reminder of the fact that broadband colours to a large degree do not reflect changes in the absorption feature strengths of the underlying spectrum, while the absorption features are tied more directly to the stellar populations in the galaxies. The different numbers of parameters in the data sets suggest that galaxies in clusters have been homogenised such that some fraction of the information from the past has been lost. Hence, it may be possible that the present-day homogeneity of early-type galaxy properties, e.g. fundamental plane relations, does not require a single formation scenario, but that a variety of formation scenarios for different galaxies could still yield the observed behaviour of nearby galaxies. Some evidence of this has been seen in the models of Shioya & Bekki (1998).

Second, the distributions of line strengths versus PC weights for the Coma and high-redshift clusters are different. One of the differences is manifest in the fact that the first principal component for Coma is dominated by metal line strengths of both light and heavy elements, while in the high-redshift clusters it is controlled by only the light elements plus the Balmer lines. One interpretation of this difference could be that the most important factor in understanding the high-redshift clusters is the prevalence of recent star formation. The correlation between Balmer lines and metal lines could then stem from the general principle of weakening metal features by adding A star light to a spectrum, although since only the light elements are involved, the reason may come from an intial post-starburst overabundance of Type II supernovae relative to Type Ia supernovae, which have a longer characteristic timescale. This could lead to large initial changes in the light elements while leaving Fe-peak elements temporarily stable. The behaviour of the first component for Coma could be demonstrating that Coma is relatively inactive in relation to the high-redshift clusters, and that the range in metallicity of the galaxies is the most relevant factor in understanding the properties of galaxies in that cluster.

The larger number of independent parameters and the importance of the Balmer lines in the high-redshift spectra suggest that we are seeing a period of relative chaos in the evolution of galaxies in rich clusters, and hence in the evolution of the clusters themselves. Perhaps the next avenue to pursue is to determine the relationship of the global properties of the clusters to the spectral properties of the galaxies. To do that will require more high-quality spectral data and morpological information in galaxy clusters over a range of redshifts.

Acknowledgments

The authors would like to thank Jim Rose and Nelson Caldwell for providing the Coma spectra, and Charley Lineweaver, Simon Driver and Michael Drinkwater for helpful discussions. This work has been supported by the Australian Research Council.

References

Caldwell, N., & Rose, J. 1997, AJ, 113, 492
Caldwell, N., Rose, J., Sharples, R., Ellis, R., & Bower, R. 1993, AJ, 106, 473
Colless, M., & Dunn, A. 1996, ApJ, 458, 435
Couch, W., Barger, A., Smail, I., Ellis, R., & Sharples, R. 1998, ApJ, 497, 188
Couch, W., Ellis, R., Sharples, R., & Smail, I. 1994, ApJ, 430, 121
Couch, W., & Sharples, R. 1987, MNRAS, 229, 423
Djorgovski, S., & Davis, M. 1987, ApJ, 313, 59
Dressler, A., Lynden-Bell, D., Burstein, D., Davies, R., Faber, S., Terlevich, R., & Wegner, G. 1987, ApJ, 313, 42
Ellis, R., Smail, I., Dressler, A., Couch, W., Oemler, A., Butcher, H., & Sharples, R. 1997, ApJ, 483, 582
Faber, S. 1973, ApJ, 179, 731
Faber, S., & Jackson, R. 1976, ApJ, 204, 668

https://doi.org/10.1071/AS98309 Published online by Cambridge University Press

González, J. 1993, PhD thesis, University of California at Santa Cruz
Gorgas, J., Faber, S., Burstein, D., González, J., Courteau, S., & Prosser, C. 1993, ApJS, 86, 153
Jones, L. 1996, PhD thesis, University of North Carolina at Chapel Hill
O'Connell, R. 1976, ApJ, 206, 370
Rose, J. 1985a, AJ, 90, 787
Rose, J. 1985b, AJ, 90, 1927
Rose, J. 1994, AJ, 107, 206
Shioya, Y., & Bekki, K. 1998, ApJ, 497, 108
Tripicco, M., & Bell, R. 1995, AJ, 110, 3035
Visvanathan, N., & Sandage, A. 1977, ApJ, 216, 214
Wood, D. 1969, AJ, 74, 177
Worthey, G. 1994, ApJS, 95, 107
Worthey, G., & Ottaviani, D. 1997, ApJS, 111, 377

https://doi.org/10.1071/AS98309 Published online by Cambridge University Press